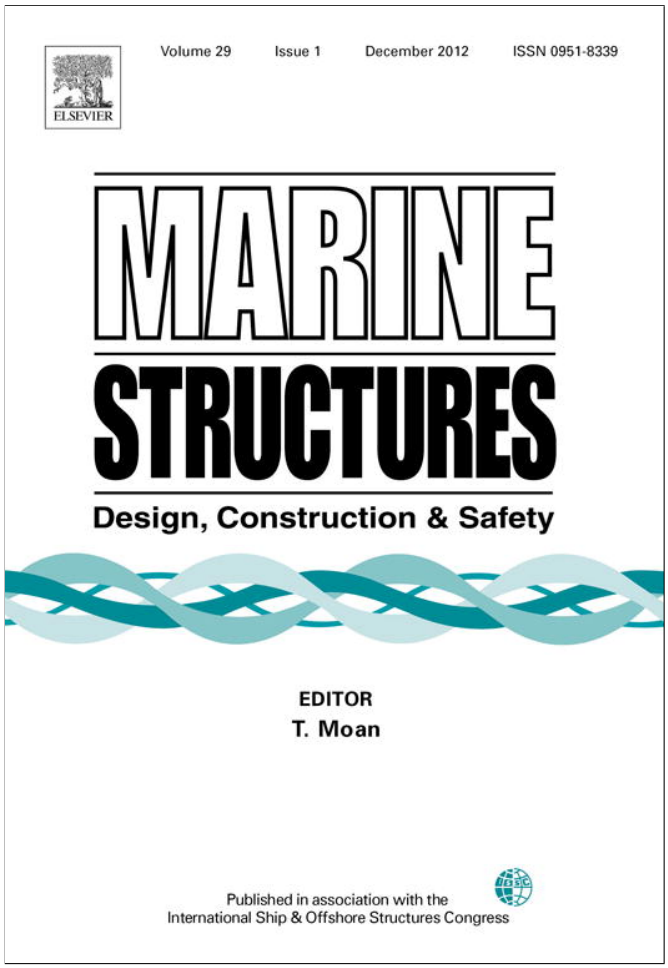

Marine Structures 29 (2012) 211–225

Contents lists available at SciVerse ScienceDirect

Marine Structures

journal homepage: www.elsevier.com/locate/marstruc

Welding stress relaxation effect in butt-jointed steel plates

Segen F. Estefen [a], Tetyana Gurova [a,b,*], Daniel Werneck [a], Anatoli Leontiev [c]

[a] Subsea Technology Laboratory, COPPE, Federal University of Rio de Janeiro, Rio de Janeiro, Brazil
[b] GURTEQ – Ensaios Não Destrutivos Ltda, Rio de Janeiro, Brazil
[c] Institute of Mathematics, Federal University of Rio de Janeiro, Rio de Janeiro, Brazil

ARTICLE INFO

Article history:
Received 6 June 2011
Received in revised form 2 June 2012
Accepted 17 June 2012

Keywords:
Residual stress
X-ray analysis
Welding
Butt joints

ABSTRACT

This paper presents an experimental study of the behavior of the residual welding stresses for butt-jointed steel plates. Two different welding processes were used to joint the plates, one with a single electrode and the other with double electrodes. The stresses were monitored over two weeks after the removal of the welding constraints. The measurements were performed at the deposited metal, the heat-affected zone, the base metal close to the weld joint and along the plate using the X-ray diffraction method and magnetic method based on the magnetostriction effect. The experimental results showed the continuous process of welding stress relaxation over a relatively short length of time with a significant difference in the final welding stress distribution from just after the removal of the welding restraints, both for the single-electrode and the double-electrode welding. The observed stress redistribution trend was characterized by a reduction in and a uniformity of the values of the maximum shear stresses. Microstructure analysis showed the absence of microcracks at the deposited metal, the heat-affected zone and the base metal close to the weld joint at the welded specimens. Thus, the possibility that the observed welding stress relaxation was the result of material failure is ruled out.

* Corresponding author. Subsea Technology Laboratory, COPPE, Federal University of Rio de Janeiro, CP 68503, CEP 21945-970, Rio de Janeiro, Brazil. Tel.: +55 21 2562 7791.
E-mail address: gurova@lts.coppe.ufrj.br (T. Gurova).

0951-8339/$ – see front matter © 2012 Elsevier Ltd. All rights reserved.
http://dx.doi.org/10.1016/j.marstruc.2012.06.002

1. Introduction

Residual stresses due to welding can significantly affect the engineering properties of materials and structural components. Metallurgical processes during welding, such as shrinkage, quenching, and phase transformations, produce both tensile and compressive residual stresses in different zones of the welded parts [1]. These residual stresses, particularly tensile stresses, can significantly impact the reliability and the integrity of the welded components. Systematic studies have shown that residual stresses may result in failure mechanisms that are sensitive to localized stresses, such as the following: fatigue, brittle fracture, stress corrosion cracking, and creep cracking. Therefore, it is important to understand the distribution of the residual stresses on the surface of the welded components in and near the welding zone.

New techniques for measurements, improvements in equipment, and advances in computational methods have stimulated both numerical and experimental studies of welding processes [2–4].

The residual stress distributions developed in welded joints and structures are difficult to predict because of the complex dependence of the residual stress field upon many different factors, such as preexisting residual stresses in the parts being joined before welding, the material properties of the weld and the jointed parts, the geometry of the parts, the applied restraints, the welding procedure, including the weld preparation, the welding conditions and the pass sequence in multi-pass welding, the residual stresses generated or relaxed by manufacturing operations after the welding or by thermal and mechanical loading during the service life. The latest studies show, for example, that the final residual welding stresses depend strongly on the clamping conditions as well, especially the clamping time, the release time and the clamp preheating [5].

In this paper, the behavior of the welding stresses was studied from the moment when the welding clamps were removed, and two different types of welding were analyzed, one with a single electrode and another with double electrodes. Double-electrode welding increases productivity because of faster deposit rates as compared with single-electrode welding. In addition, the heat input to the base metal can be maintained relatively low for double-electrode welding, while the conventional single-electrode gas metal arc welding (GMAW) uses a large current for a high deposition rate. Therefore, for the same deposition rate, the double-electrode process is associated with less heat and a low base metal current as compared with the single-electrode GMAW. Many of the different characteristics of double-electrode welding have already been investigated, such as the process stability, the effects of the total current, the melting rate, the microstructure, and the heat affected zone (HAZ) hardness [6–8]. Single-electrode and double-electrode welding stress distributions are expected to be different because of their respective thermal regimes, thermal cycles, thermal front extensions, cooling regimes, quantity of melted material and, consequently, the effects of the phase transformations that occur in the deposited metal, the HAZ, and the base metal close to the weld fillet [7].

It is noted that the authors of measurement experiments almost never specify exactly how long after the removal of the clamps the welding stress measurements were performed. However, the numerical results of welding stress simulations correspond to the moment just after the cool down or the removal of the clamps. Thus, the authors that compare numerical and experimental welding stress results probably suppose that the welding stress distributions will not change with time upon completion of the welding procedure. Our experiments show over a relatively short length of time, two weeks after the removal of the clamps, the welding stress distribution undergoes a notable transformation, and the stresses only stabilize at the end of this process. This stress relaxation process is probably one of the reasons explaining the differences reported by some authors between the results of experimental welding stress measurements and the welding stresses estimated by computer simulations [9].

2. Experimental arrangement

The experiments were performed using ASTM A131 grade A ferrite steel plates typically employed in the shipbuilding industry. The nominal yield strength of the plate material was 235 MPa, and the chemical composition is presented in Table 1. For each test, two plates were jointed with dimensions 1200 mm $\times$ 500 mm $\times$ 19 mm and a chamber angle of 20° (see Fig. 1). Specially designed tables were

Table 1
Chemical composition of material of the plate.

Element	Quantity (%)
Carbon	0.23
Iron	97.0
Manganese	2.73
Phosphorus	0.035
Sulfur	0.040

manufactured in order to support the plates and to provide the clamped conditions during the welding. The plates were restricted from out-of-plane displacements along the outside edges as shown in Fig. 2. The welding constraints were removed one day after welding.

The first pair of plates was jointed using single-electrode welding in four filling layers and 11 steps using the Metal Inert Gas (MIG) manual procedure with a rod feeding speed of 8 m/min. The average values of the welding current and the voltage were 211 A and 24.1 V, respectively. The second pair of plates was welded using the double-electrode technique in three steps. The first two steps deposited 11 mm welds and the third, a 17 mm weld. The welding procedure was performed automatically by a welding machine with tandem arc as shown in Fig. 2. Welding data are presented in Table 2. For both cases, the employed electrode was a 1.2 mm carbon steel rod, Supercored 70NS, identified by the specification AWS A5.18/ASME SFA5.18 E70C-6M with a yield strength of 440 MPa.

3. Stress measurement methodology

The absolute values of the stresses were measured on the top side of the plate surface by the X-ray diffraction method using the portable equipment RAYSTRESS, which employs the method of double exposure [10]. This measuring technique has been widely tested and successfully employed in many different practical engineering applications [11–17].

The principle of the stress measurements is demonstrated in Fig. 3. Two cassette windows capture the diffraction lines in 2θ angular intervals from 148° to 164°. Inclination of the specimen surface of 12° corresponds to measurements for steel specimens using Cr-K_α radiation and {211} reflection with $\theta_{211} = 78°$.

When using the X-ray diffraction method to measure weld stresses, some authors pay special attention to the stress-free lattice spacing. The hypothesis that the change of this lattice spacing across the weld due to microstructural variations affects the results of the stress measurements has been explored, for example, in the paper [18]. To adjust the experimental stress measurement results, a least squares optimization problem is solved by considering the unstrained lattice spacing as a control parameter. The optimal solution guarantees that the measured stress is close to the theoretically predicted value at a certain set of measurement points. Then, the obtained optimal lattice spacing is used to recalculate the stress at the rest of the measurement points. However, experimental results [19]

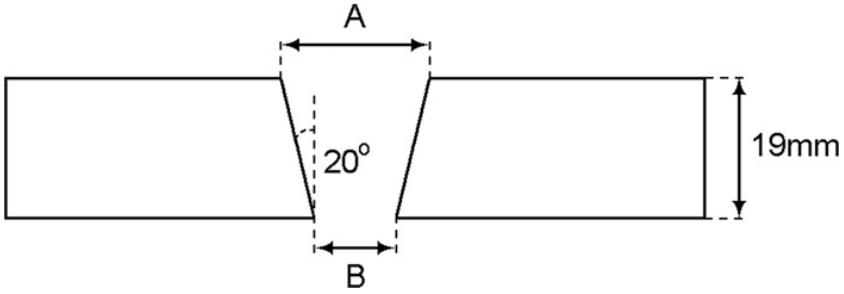

Fig. 1. Chamber details. Single-electrode welding: $A = 20$ mm, $B = 6$ mm; Double-electrode welding: $A = 18$ mm, $B = 4$ mm.

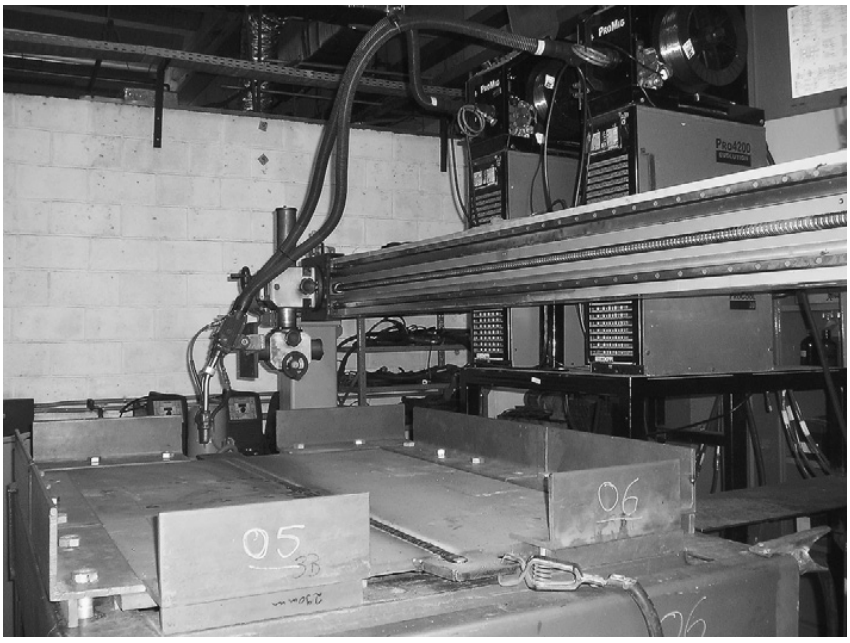

Fig. 2. Plates fixed by clamps along the edges on the support table and automatic double-electrode welding machine.

have shown that there is no significant variation of the stress-free lattice spacing, and thus, we assume here that the interplanar distance d_0 does not change across the weld.

Portable magnetic equipment is used to map the stresses in and around the neighborhood of the weld. The device employs the inverse effect of magnetostriction with a MAS type sensor (magnetic anisotropic sensor). The inverse effect of magnetostriction relies on the variation in the magnetic response of the metal when subjected to the mechanical stresses because of a change in the magnetic domains. The first work concerning the practical use of this technique dates back to the 1960s [20]. Additionally, we should mention the results of the Japanese school of the 1990s [21,22].

The MAS sensor used in this study has two coils in a U shape positioned orthogonally. One coil is responsible for the induction (magnetization), while the other is used for detection (see Fig. 4). The induction coil produces an electromagnetic wave that passes through the material, generating a reflected wave that is captured by the detection coil. For a sine wave with a magnetic field intensity of H_0 and a frequency ω transmitted in the z direction, which is orthogonal to the metal surface, the intensity of the magnetic field H at depth z in a ferromagnetic material with magnetic permeability μ is given by

$$H = H_o * \exp(ikz),$$

Table 2
Double-electrode welding data.

Pass	Electrode	U (V)	I (A)	Welding speed (cm/min)
1	1	28.0	325.0	30.0
1	2	25.2	244.0	30.0
2	1	30.6	373.0	30.0
2	2	28.6	280.0	30.0
3	1	33.6	361.0	30.0
3	2	32.6	270.0	30.0

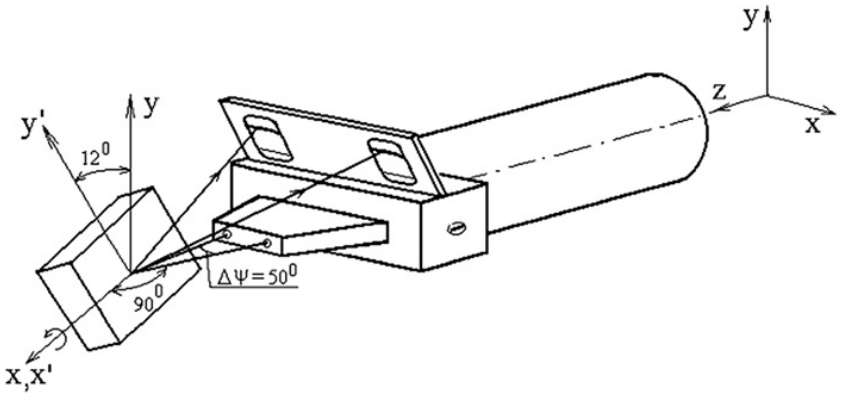

Fig. 3. Scheme of stress measurements with RAYSTRESS equipment.

where $k = (i + 1/\delta)$ and $\delta = C\sqrt{2\pi\mu\omega}$. The angle α between the direction of H and the principal direction of the mechanical stress is set to be 45°. The magnetic flow registered by the detection coil is proportional to the component of the magnetic induction vector B in the direction between the coil poles. The electromotive force induced in the detection coil is given by

$$dU = M(B_x - B_y)\exp(ikz)dz,$$

where M is a coefficient that characterizes the material properties of the metal being analyzed. Integrating over the thickness h, the signal captured by the detection coil can be found by the following:

$$U = \frac{MH}{2}\int_0^h \Big(\mu_x(z) - \mu_y(z)\Big)\exp(2ikz)dz.$$

The magnetic permeabilities in both the longitudinal μ_x and the transverse directions μ_y vary with the mechanical stress σ. This variation is proportional to σ and is given by $\mu_x - \mu_y = \beta^*\sigma$, where β is a material constant. Therefore, the voltage captured by the sensors is given by the following:

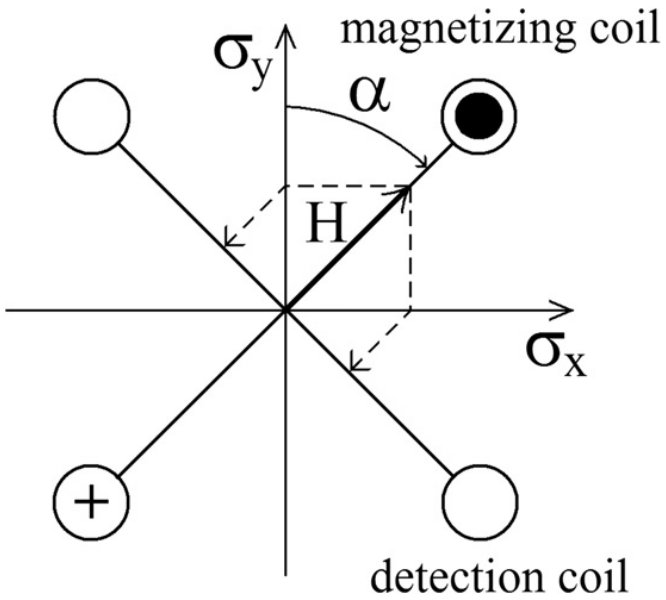

Fig. 4. Operation scheme of MAS type sensor.

$$U = A\int_0^h \sigma(z) * \exp(2ikz)dz,$$

where A is a specific constant of the sensor. In this way, the sensor registers the value σ_{reg} of the demodulation in the amplitude of the wave with frequency ω as follows:

$$\sigma_{reg} = \frac{\int_0^h \sigma(z)\exp(2ikz)dz}{\int_0^h \exp(2ikz)dz},$$

The value σ_{reg} is then used to find the difference between the principal stresses, the modulus of which is equal to twice the value of the maximum shear stress. The value of the maximum shear stress is utilized directly in the Tresca-Guest yield criteria.

4. Experimental results

The X-ray residual stress measurements for each pair of joined plates were performed along the mid-plate perpendicular to the weld line at four different points (1–4) spaced 50, 100, and 150 mm from each other as well as at the points along the deposited metal (WM), the heat-affected zone (HAZ) and the base metal close to the weld fillet (BM). The BM point was spaced 10 mm from the HAZ point, and point (1) was spaced 10 mm from the BM point. At each point, the stresses were measured in two directions, parallel to the weld (longitudinal stress σ_{L}) and perpendicular to the weld (transverse stress σ_{T}). Electro-chemical etching to a depth of 0.2 mm was applied both to guarantee the absence of mechanical stress induced on the plate surface by manufacturing or collateral procedures and to identify the limits of the HAZ. Registration of {211} diffraction lines with the Cr–Ka wavelength were used for the X-ray analysis. The magnitudes of the X-ray elastic constants were taken from [23]. The beam spot dimensions were 0.5 mm $\times$ 6 mm. The experimental accuracy of the stress measurements was 20 MPa. Measurements of the stresses in arbitrary directions in the plates before welding showed the presence of residual tensile stresses between 20 and 40 MPa caused by the thermo-mechanical treatments of the plates during fabrication.

The magnetic method measurements were performed over an area of 90 mm by 45 mm at 190 points of a rectangular mesh with a uniform step of 5 mm. The area was centered above the weld line and the mid-plate at the top side of the plate. The largest side of the area was perpendicular to the weld line. First, it should be noted that the mapping was performed over an area composed of materials with different mechanical and magnetic properties (the weld metal, the base metal and probably the heat-affected zone). Thus, the measurements are relative for each part of the mapped area. Second, the mapped area contained more measurement points than the X-ray analyses. Third, the magnetic method provided an average measurement to a depth of 3 mm, while the X-ray results correspond to the superficial stress values. For these reasons, we used these measurements to form maps of the maximum shear stress concentration and, moreover, for an independent comparison.

The stress measurements were performed one day after welding with the imposed welding constraints, two days after welding and two weeks after welding. During the two weeks period the welded plates remained on the support table at the laboratory conditions and ambient temperature from 26 to 30 °C.

4.1. Single-electrode welding results

Over the two week period, reductions in the longitudinal stresses σ_{L} at the measuring points of the weld metal and the heat-affected zone were observed. These decreases were accompanied by an increase in the stresses at the base metal measuring points as compared with the two-day distribution (see Fig. 5).

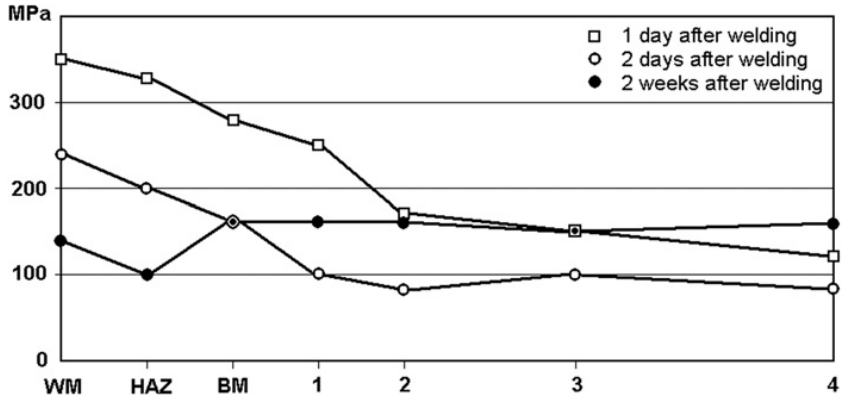

Fig. 5. Absolute values of longitudinal stresses σ_L for single-electrode welding.

For the transverse stresses σ_T, the values at the measuring points of the heat affected zone and the base metal close to the weld fillet increased after 2 weeks as compared with the two-day distribution (see Fig. 6).

A fuller picture of the welding stress relaxation emerged as the maximum shear stress redistribution was observed. Additional measurements at each measuring point directed at a 45° angle with respect to the used measuring directions show that the stresses measured in the longitudinal and the transverse directions were the principal stress directions near the weld fillet and are close to the principal stress directions at the other measuring points. This result is expected from a theoretical point of view due to symmetry, and it allows us to obtain the maximum shear stress values τ_{max} as a half of the modulus of the difference between the measured stresses in the longitudinal and the transverse directions (see Fig. 7).

For the single electrode welding, the two-week welding stress state was characterized by a more uniform distribution of the maximum shear stresses but with a lower absolute value than for the constrained and two-day welding stress distribution. It is interesting to note that the maximum shear stress obtained for the two-day distribution was greater than the constrained weld state close to the weld fillet (the HAZ and the BM points). Thus, from the Tresca yield criteria standpoint, the two-week

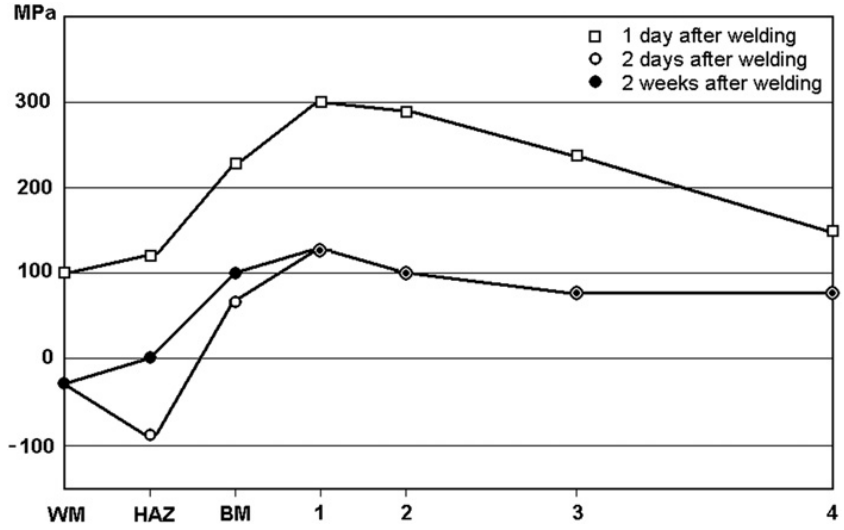

Fig. 6. Absolute values of transverse stresses σ_T for single-electrode welding.

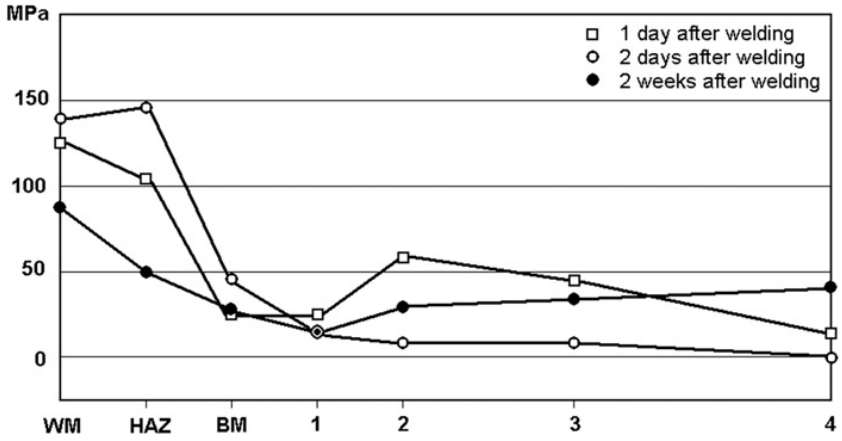

Fig. 7. Absolute values of maximum shear stresses τ_{max} for single-electrode welding.

welding stress state was less critical than that of the two-day state. For these reasons, the observed welding stress redistribution can be associated with the relaxation of the welding stress.

The same trend was observed for the mapping of the concentration of the maximum shear stresses obtained by the magnetic method. The maximum concentration of shear stresses α_i at the measuring point i is described by the following formula:

$$\alpha_i = \frac{\tau_i}{\frac{1}{N}\sum_{j=1}^{N}\tau_j},$$

where τ_i (τ_j) is the relative value of the maximum shear stresses measured at the point i (point j) and N is the number of measuring points. The maximum value of the stress concentration for the two-day plates (equal to 9.0) is greater than that stress concentration for the two-week plates (equal to 6.5) (see Fig. 8).

4.2. Double-electrode welding results

For the two-day stress distribution for the double-electrode case, in Figs. 9 and 10, higher and more uniform stresses were observed than for the single-electrode case, especially in the longitudinal direction. For the double-electrode case, the initial distribution (clamps imposed) of the maximum welding stress values in the longitudinal directions were found at both the HAZ and the base metal close to the fillet, while for the single-electrode case, the maximum welding stress values were located along the deposited metal. As a consequence, the welding stress after two days in the double-electrode case had a different distribution from that obtained from the single-electrode welding. For the single-electrode case, the two-day residual stress distribution resulted from the stress redistribution on the deposited metal. For the double-electrode case, the stress reduction in the base metal close to the fillet resulted in an increase of the stresses on the weld metal in the longitudinal direction. Similar trends were observed in the other experiments involving double-electrode welding [24].

Comparing the two-week stress distribution with two-day one, it can be noted that after two weeks, a reduction of the longitudinal stresses at all measuring points and a reduction of the transverse stresses of the weld metal and the heat affected zone were accompanied by an increase in the stresses at the measuring points remotely positioned from the weld fillet.

Similar to the single-electrode case, for the double-electrode welding, the two-week welding stress state was characterized by a more uniform distribution of the maximum shear stresses but with smaller absolute values than that for the constrained and two-day welding stress distribution (see Fig. 11). It is interesting to note that the maximum shearing stress obtained from the two-day

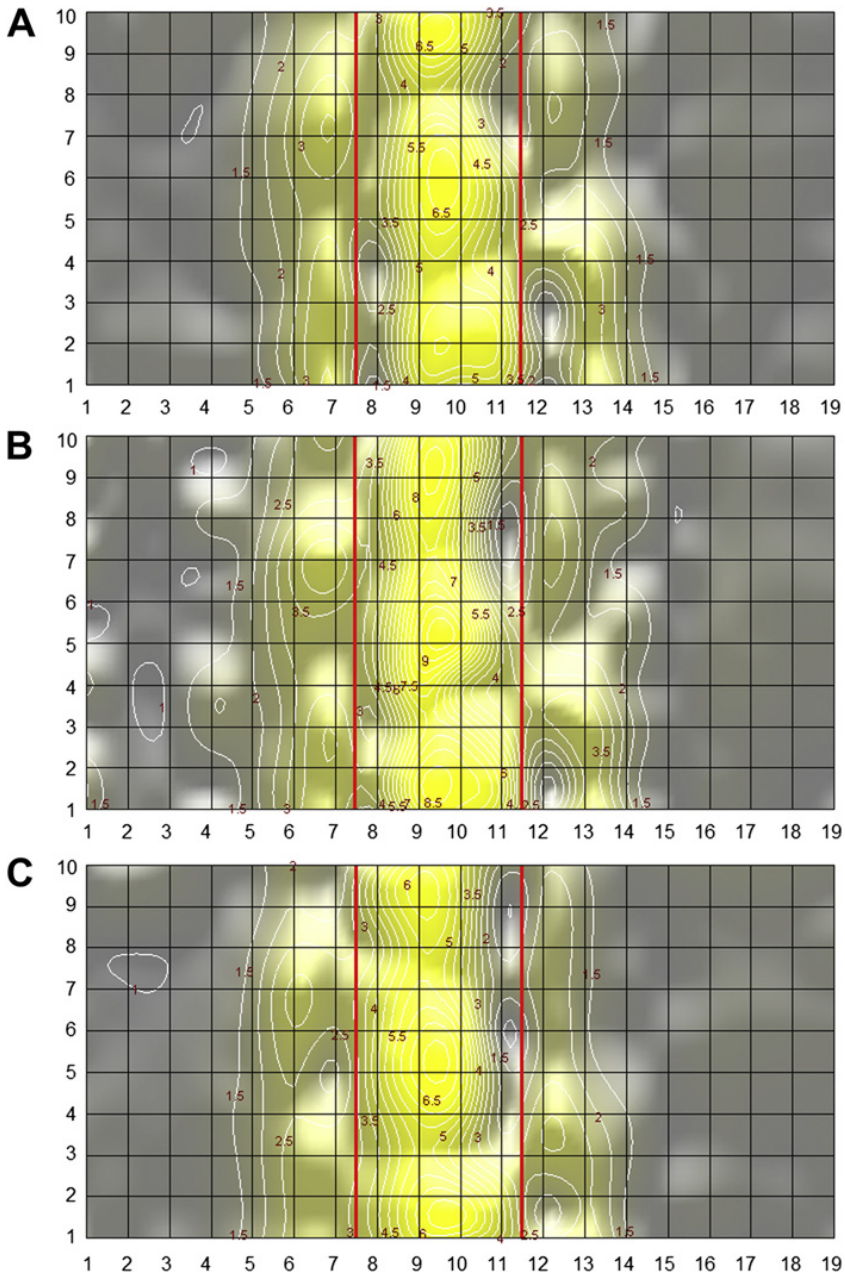

Fig. 8. Single-electrode welded plate. Maps of maximum shear stress concentration at the area close to the weld fillet. A – one day after welding, clamps imposed; B – two days after welding and one day after clamp removal; C – two weeks after welding. Step of level curves is 0.5. Vertical red lines mark the weld position.

distribution was, except on the HAZ measuring point, of greater or equal value to all other stresses, even when compared with the constrained weld state.

No significant difference was observed in the mapping of the maximum shear stress concentration as was observed for the single electrode (see Fig. 12). This finding probably corresponds to the fact that the graphs for the absolute value of the shear stress for two days and two weeks had relatively similar profiles.

4.3. General comparison

The two week period was chosen experimentally based on the results of the measured stresses. It was noted that after this period, the values of the measured stresses did not change. However, it is not possible to confirm that this is the minimum necessary time for the relaxation of the residual stresses.

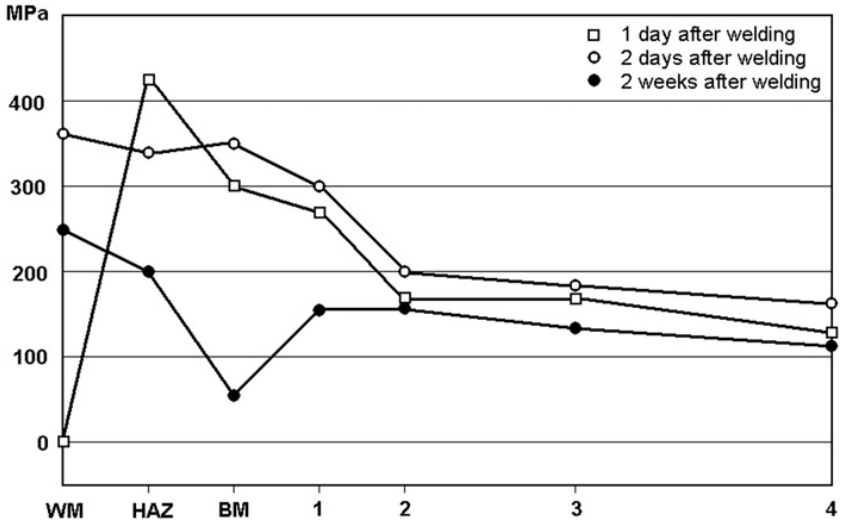

Fig. 9. Absolute values of longitudinal stresses σ_L for double-electrode welding.

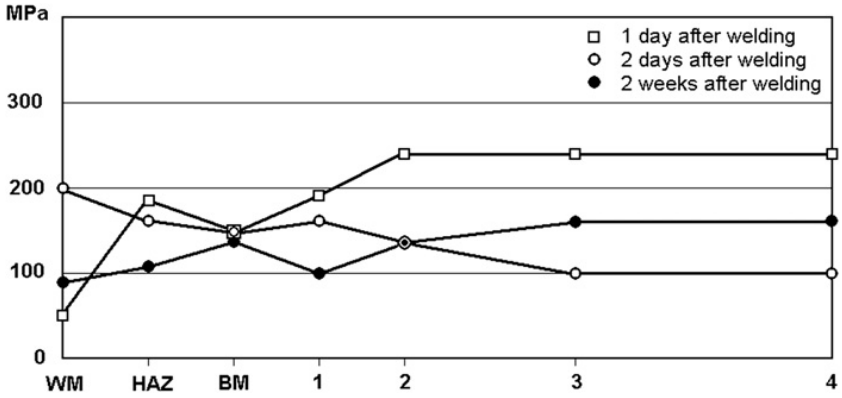

Fig. 10. Absolute values of transverse stresses σ_T for double-electrode welding.

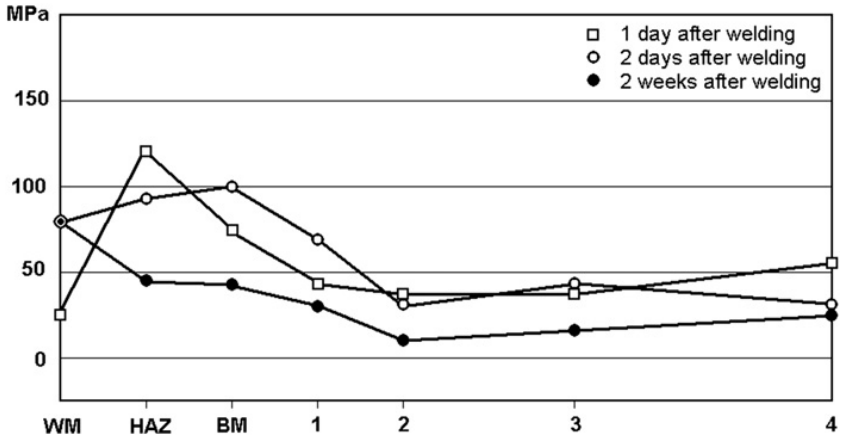

Fig. 11. Absolute values of maximum shear stresses τ_{max} for double-electrode welding.

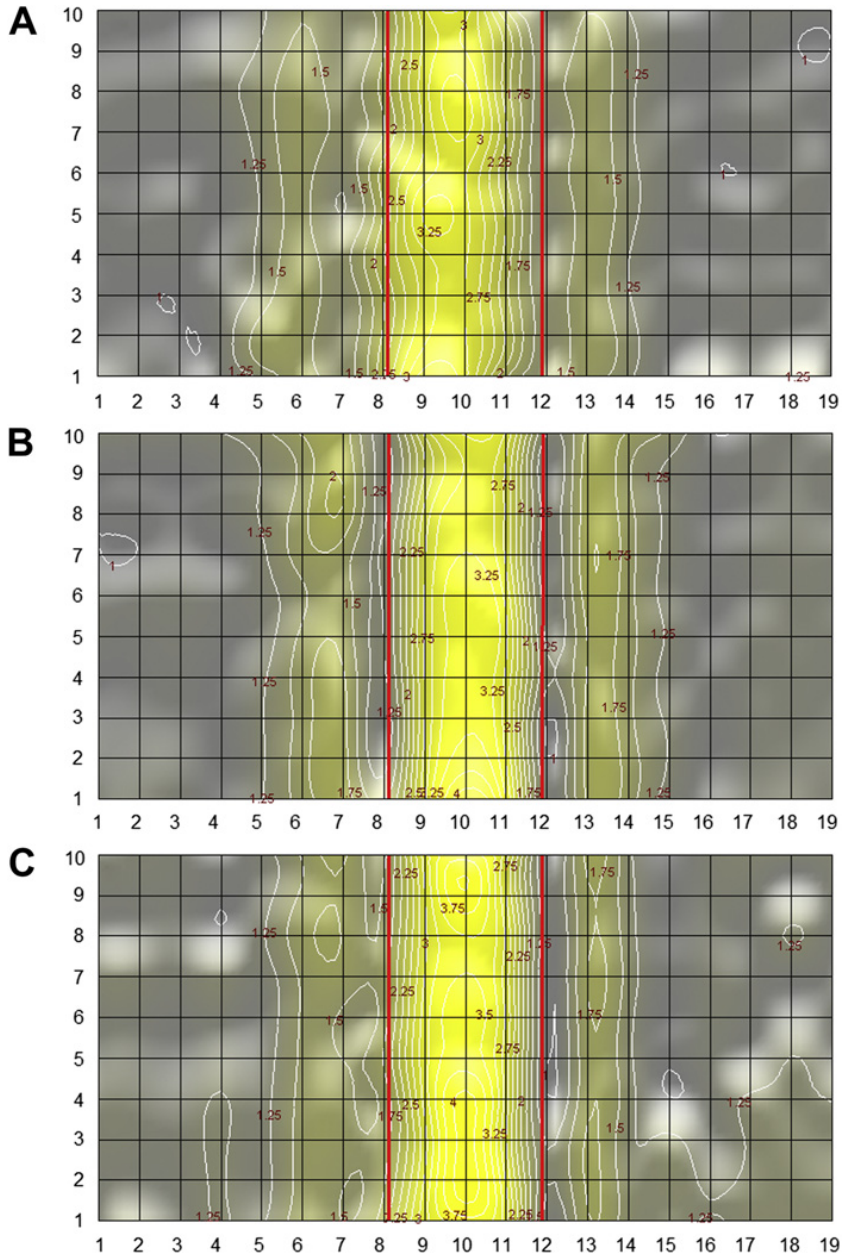

Fig. 12. Double-electrode welded plate. Maps of maximum shear stress concentration at the area close to the weld fillet. A – one day after welding, clamps imposed; B – two days after welding and one day after clamp removal; C – two weeks after welding. Step of level curves is 0.25. Vertical red lines mark the weld position.

Even so, significant changes in the results of the measured stress distributions after two days and two weeks were observed for all the processes. Additionally, a similarity was observed in the distributions of the final values of the absolute maximum shear stresses for both the single- and the double-electrode welding after two weeks, although they were different when compared with two days after welding (see Figs. 13 and 14). The observed stress redistribution trend is characterized by the reduction and the uniformity of the values of the maximum shear stresses.

5. Metallographic examination

A $10 \times 60 \times 19$ mm cross section of the weldments composed of the parent plate and the weld metal was removed transverse to the welding direction to produce specimens for examination of the

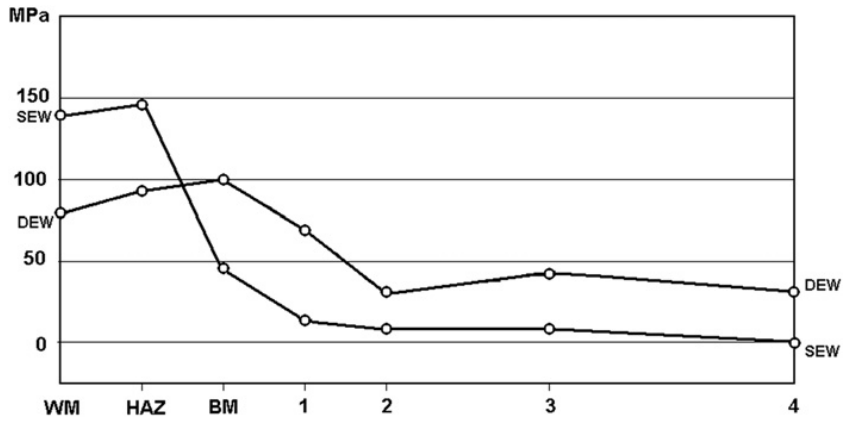

Fig. 13. Absolute values of maximum shear stresses τ_{max} for single-electrode (SEW) and double-electrode (DEW) welding in 2 days.

microstructure. The weld metal microstructure was revealed using 2% Nital. The microstructure was evaluated using a standard optical microscope.

Fig. 15(A) shows in detail the microstructure of the random areas of the weld bead for a single-electrode weld. The refined microstructure contained perlite and dispersed cementite particles in a ferrite matrix. This microstructure resulted from the recrystallization of the deposited metal because of the subsequent pass. Fig. 15(B) presents the microstructure of the deposited metal for the finishing pass of the double-electrode weld. The microstructure was composed of ferrite in a dentritic columnar arrangement containing carbine particles. The original image is presented at a 200× magnification. Fig. 16(A) shows the general aspect of the heat-affected zone microstructure close to the finishing pass for the single-electrode weld. A ferrite matrix with cementite in a cellular arrangement was present. Fig. 16(B) displays the same area for the double-electrode weld. The original image is presented at a 100× magnification.

The base metal microstructures of the analyzed samples for both the single- and the double-electrode weld were typical structure of a carbon steel plate comprised of ferrite light areas and perlite dark areas with a grain size of ASTM 8. Examples of this type of microstructure are presented in Fig. 17(A) and (B) for the single- and the double-electrode jointed plates, respectively. The image is presented at a 100× magnification.

The microstructure analysis demonstrated the absence of microcracks in the deposited metal, the heat affected zone and the base metal close to the weld joint on the welded specimens. Thus, the possibility that the observed welding stress relaxation was the result of material failure can be ruled out.

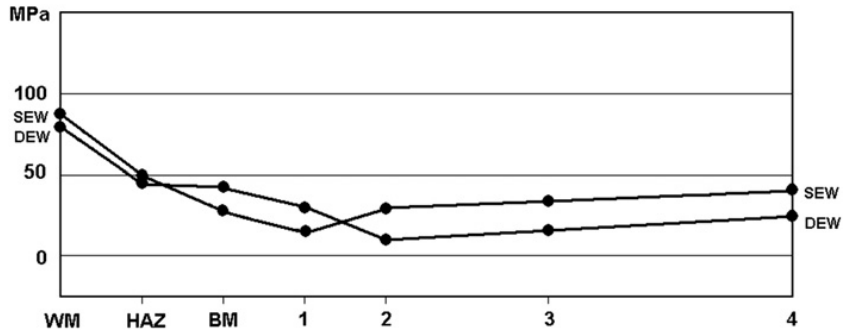

Fig. 14. Absolute values of maximum shear stresses τ_{max} for single-electrode (SEW) and double-electrode (DEW) welding in 2 weeks.

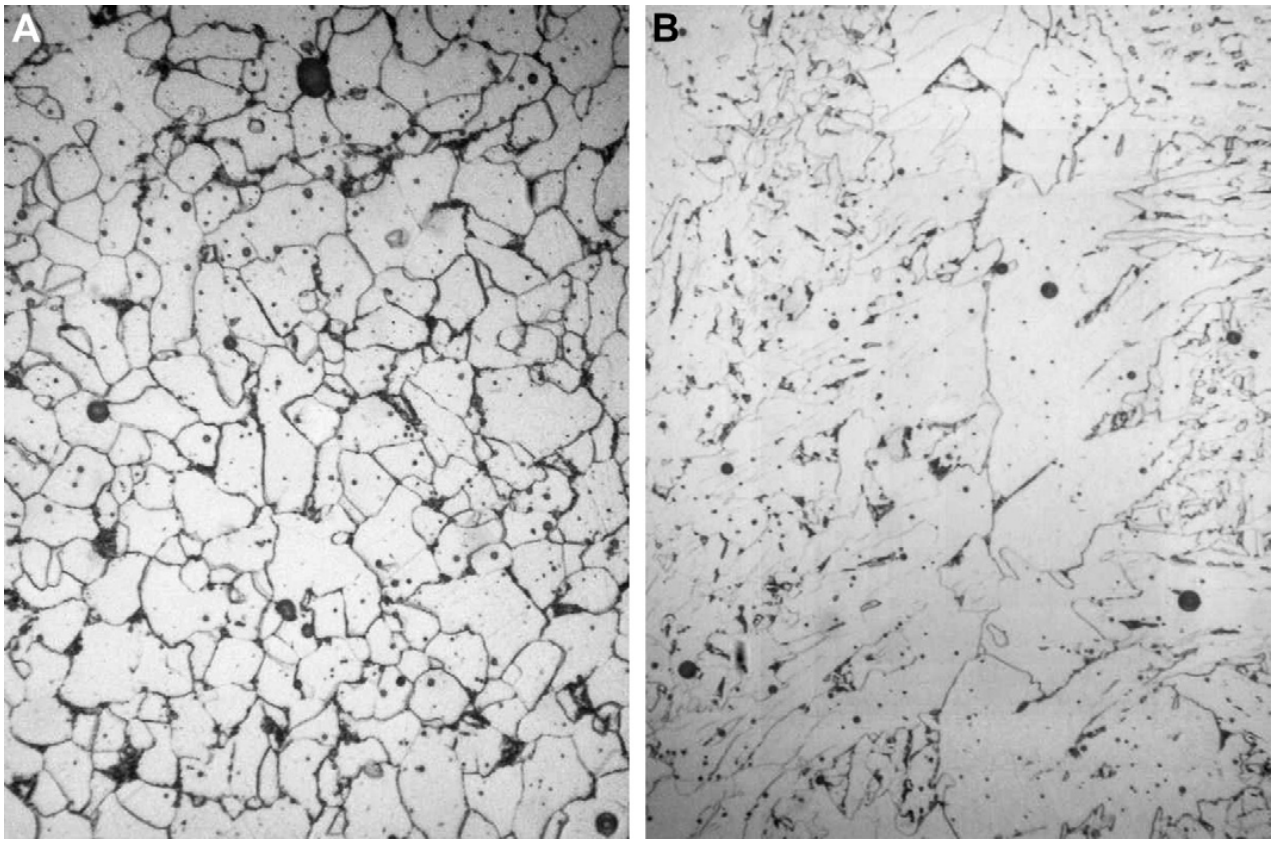

Fig. 15. Deposited metal microstructure. (A) – Single-electrode weld. (B) – Double-electrode weld. Amplification is 200 times.

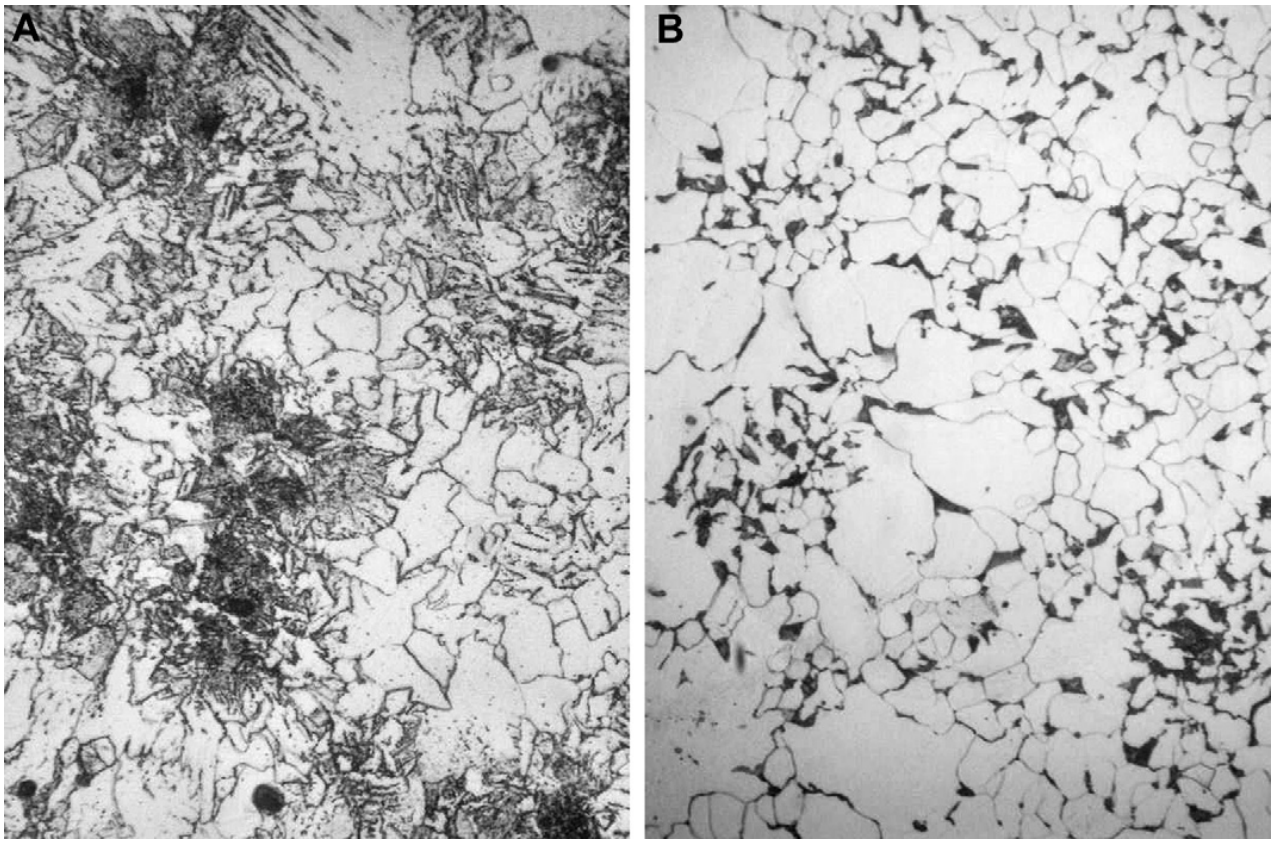

Fig. 16. Heat affected zone microstructure. (A) – Single-electrode weld. (B) – Double-electrode weld. Amplification is 100 times.

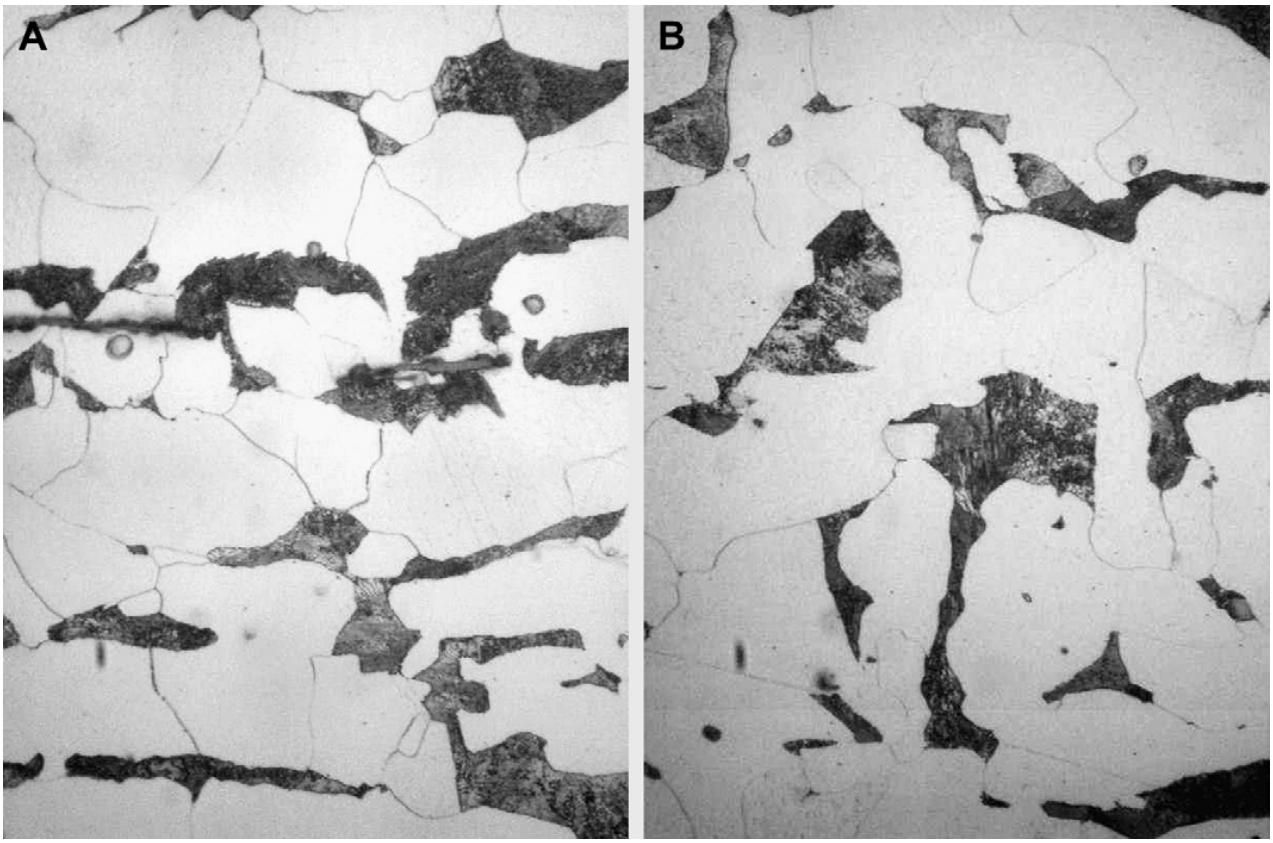

Fig. 17. Base metal microstructure. (A) – Single-electrode weld. (B) – Double-electrode weld. Amplification is 100 times.

6. Conclusions

1. The experimental results obtained with two different techniques showed that the welding stress distribution for the butt-jointed steel plates underwent notable transformation over a period of two weeks after the completion of the welding procedure both for the single-electrode and the double-electrode welding techniques.
2. The final (two-week) welding stress state was characterized by a more uniform distribution of the maximum shear stresses with smaller absolute values than that for the constrained and initial (two-day) welding stress distribution.
3. The microstructure analysis of the welded specimens ruled out the possibility that the observed welding stress relaxation might be the result of material failure.
4. It seems to be reasonable for the welding stress measuring results to specify the moment of measuring upon completion of the welding procedure.
5. The effect of the welding stress relaxation observed in the experiments has the potential to provide a very significant improvement in the interpretation of experimental data for the purpose of residual stress assessment.
6. The period of the welding stress relaxation, observed during the reported experiments, and its final distribution probably depends on both the type and the conditions of the welding, including the geometry (and the dimensions) of the welded specimen. Therefore, it would be interesting to study this relationship to find the minimum time necessary to complete the relaxation of the stresses for each welding technique.

Acknowledgments

This work was supported by FINEP/Brazilian Ministry of Science and Technology and TRANSPETRO/PETROBRAS. The assistance of White Martins S.A. with double-electrode welding is gratefully

acknowledged. Special thanks to the technical team from the Subsea Technology Laboratory – COPPE/UFRJ. The first author (S.F.E.) gratefully acknowledges the support provided by CNPq (Conselho Nacional de Desenvolvimento Científico e Tecnologico, Brazil) research grant N 302531/2009-2. The last author (A.L.) also acknowledges the CNPq for the research grant N 305338/2009-9.

References

[1] Macherauch E, Wohlfahrt H. Different sources of residual stress as a result of welding. In: Nichols RW, editor. Residual stress in welded construction and their effects: an international conference, 1977 Nov 15–17. London, Cambridge: Welding Institute; 1978–1979. p. 267–82.
[2] Gannon L, Liu Y, Pegg N, Snith M. Effect of welding sequence on residual stress and distortion in flat-bar stiffened plates. Mar Struct 2010;23:385–404.
[3] Paradowska AM, Price JWH, Finlayson TR, Lienert U, Walls P, Ibrahim R. Residual stress distribution in steel butt welds measured using neutron and synchrotron diffraction. J Phys Condens Matter 2009;21(12):8.
[4] Deng D, Murakawa H. Prediction of welding distortion and residual stress in a thin plate butt-welded joint. Comput Mater Sci 2008;43:353–65.
[5] Schenk T, Richardson IM, Kraska M, Ohnimus S. A study on the influence of clamping on welding distortion. Comput Mater Sci 2009;45:999–1005.
[6] Li K, Zhang YM. Metal transfer in double-electrode gas metal arc welding. J Manuf Sci Eng 2007;129:991–9.
[7] Li KH, Zhang YM. Consumable double-electrode GMAW – part 1: the process. Weld J 2008;87:11–7.
[8] Li KH, Zhang YM, Xu P, Yang FQ. High-strength steel welding with consumable double-electrode gas metal arc welding. Weld J 2008;87(Suppl):S57–87.
[9] Aloraier A, Al-Mazruoee A, Price JWH, Shehata T. Weld repair practices without post weld heat treatment for ferrítica alloys and their consequences on residual stresses: a review. In J Press Vessel Pip 2010;87:127–33.
[10] Monin V, Teodosio JR, Gurova T. A portable X-ray apparatus for both stress measurements and phase analysis under field conditions. Adv X-ray Anal 2000;43:66–71.
[11] Gurova T, Teodosio JR, Rebello JM, Monin V. Study of the residual stress state during plastic deformation under uniaxial tension in a 5.0Cr and 0.5Mo steel. Scr Mater 1997;36:1031–5.
[12] Gurova T, Teodosio JR, Rebello JM, Monin V. Variation of the residual stress state in a welded joint during plastic deformation in a 5.0% Cr and 0.5% Mo steel. J Strain Anal Eng Des 1997;32:455–9.
[13] Gurova T, Teodosio JR, Rebello JM, Monin V. Model for the variation of the residual stress state during plastic deformation under uniaxial tension. J Strain Anal Eng Des 1998;33:367–72.
[14] Monin V, Teodosio JR, Gurova T, Assis J. X-ray study of the inhomogeneity of surface residual stresses after shot-peening treatment. Adv X-ray Anal 2000;43:48–53.
[15] Monin V, Teodosio JR, Gurova T. Study and service control of stress state of high-strength steel cables used in prestressed concrete structures. Adv X-ray Anal 2001;44:195–200.
[16] Monin V, Teodosio JR, Gurova T. Analysis of residual stress state in speed gears for automotive vehicles. Adv X-ray Anal 2001;44:187–94.
[17] Assis JT, Monin V, Teodosio JR, Gurova T. X-ray analysis of residual stress distribution in weld region. Adv X-ray Anal 2002; 45:225–31.
[18] Korsunsky AM, Regino GM, Nowell D. Variational eigenstrain analysis of residual stresses in a welded plate. In J Solids Struct 2007;44:4574–91.
[19] Paradowska A, Finlayson TR, Price JWH, Ibrahim R, Steuwer A, Ripley M. Investigation of the samples for residual strain measurements in a welded specimen by neutron and synchrotron X-ray diffraction. Phy B 2006;385–386:904–7.
[20] I-39–63Handbook of control of quality by electroacoustic, radiometric and magnetic methods. Leningrad: Leningradstroy; 1962 [in Russian].
[21] Abuki S. Effects of surface conditions on residual stress measurement by magnetic probe. In: Tanaka KP, editor. Proceedings of the third international conference on residual stresses, ICRS 3, 23–26 July 1991. Tokushima, Japan: 1992. p. 1081–6.
[22] Lu J, editor. Handbook of measurement of residual stresses. Liburn: The Fairmont Press Inc; 1996.
[23] Hauk V. Structural and residual stress analysis by nondestructive methods, evaluation –application – assessment. Amsterdam: Elsevier Science; 1997.
[24] Estefen SF, Gurova T, Castello X, Leontiev A. Surface residual stress evaluation in double-electrode butt welded steel plate. Mater Des 2010;31:1622–7.